Spatial Statistics 69 (2025) 100920

Contents lists available at ScienceDirect

Spatial Statistics

journal homepage: www.elsevier.com/locate/spasta

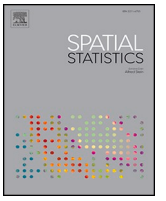

Geographically informed graph neural networks

Xuankai Ma [a,*,1], Zehua Zhang [b,1], Yongze Song [b]

[a] Urumqi Urban Institute of Geotechnical Investigation Surveying and Mapping, Urumqi 830011, PR China
[b] School of Design and the Built Environment, Curtin University, Perth 6102, Australia

ARTICLE INFO

Keywords:
GIGNN
Spatial statistic trinity
Spatial heterogeneity
Spatial features
Graph neural networks

ABSTRACT

Graph neural networks (GNNs) have been introduced to spatial statistical tasks due to their mechanisms of simulating spatial interactions and processes among geographical neighbours using graph structures. However, previous methods ignore quantifying differences in attributes among adjacent spatial characteristics. Considering this spatial characteristic by fitting the spatial statistic trinity (SST) framework may help improve models' accuracy and robustness. Thus, we introduce the geographically informed graph neural network (GIGNN) by considering the additional geospatial feature: closer geographical entities may interact less when spatial disparities are captured. When setting up the model, GIGNN leverages differences of attributes by spatial stratified heterogeneity, quantifies connections between geographical entities, and inherits k-order neighbour attribute aggregation and message-passing mechanisms from GNNs. GIGNN is applied to an urbanization analysis study in the Greater Perth Area, Australia, showing higher accuracy than the existing machine learning models and other GNNs in simulation and prediction accuracy. GIGNN achieved an accuracy of 84.1% for simulation and an accuracy of 81% for prediction. Incorporating spatial characteristics into GNNs enhances simulation and prediction accuracy in geoscientific applications, highlighting the importance of spatially aware models in solving complex problems by capturing geographical data dependencies.

1. Introduction

Geospatial artificial intelligence (GeoAI) has been introduced into human geography fields with solid methodological and theoretical development in recent years (Hu et al., 2023; Reichstein et al., 2019; Wang and Biljecki., 2022). These methods have been applied to practical human geography studies in built environment and infrastructure management (Swietek and Zumwald, 2023), land use analysis (Gevaert and Belgiu, 2022; Wang and Brenning, 2023), and human activity monitoring (Jin et al., 2023) due to the capability of big data processing and high accuracy (Song et al., 2023). Deep learning approaches using neural network structures, one of the most essential branches of AI methods, support geospatial analysis tasks, such as classification, simulation, and prediction (Liu et al., 2022; Xu et al., 2023). These statistical machine learning models include different forms of artificial neural network (ANN) structures with multiple layers and many nodes representing neurons trained from raw inputs after capturing features of targets (Zhu et al., 2020). Current AI methods require additional interpretability (Barredo Arrieta et al., 2020) and transparency (Iyer et al., 2018; Xing and Sieber, 2023), while the capability and performance of these methods for spatial data analytics can also be enhanced by simulating spatial processes, structures, and other geographical data characteristics.

* Corresponding author.
E-mail address: maxuankai20@mails.ucas.ac.cn (X. Ma).
[1] Their contributions to this work were equally significant.

https://doi.org/10.1016/j.spasta.2025.100920
Received 25 November 2024; Received in revised form 10 May 2025; Accepted 14 July 2025
Available online 15 July 2025

GNNs as deep learning methods in GeoAI have been introduced to quantitative studies of geography, including but not limited to Earth Observations (Ding et al., 2021), urban built environment analysis (Liu et al., 2023), and urban prediction (Zhu et al., 2020), due to their simulations on spatial processes using graph-based representations for spatial entities. The graph-based structures in GNNs can well represent spatial interactions and connections from each spatial unit to its associated neighbors and the geography law of spatial autocorrelation (Zhu et al., 2022). However, GNNs also face challenges in spatial modeling. These include mapping geographical entities or phenomena to graph topology while preserving the multidimensional spatial data characteristics, selecting effective GNN architectures and operating mechanisms for spatial scenario modeling, and maintaining good performance in spatial prediction and mapping tasks. (Jiang, 2020; Wu et al., 2020).

It is also believed that better simulation results from the modelling process guided by domain knowledge can lead to better results (Dikmen and Burns, 2022). In spatial data science, apart from the first law of geography, other characteristics of spatial data can also be implemented in AI-based methods for better model performance (Zhang et al., 2023). The conventional approach of conceptualizing spatial connectivity relationships using single-dimensional features applied to global modeling significantly loses local spatial relationship details. Such limitations directly impede the accuracy and stability of spatial predictions in these models. Recent studies, such as those by Islam et al. (2022) and Samek et al. (2021), emphasize the need for advanced methodologies in spatial analysis with machine learning and deep neural networks.

Spatial stratified heterogeneity (SSH), as a form of spatial non-stationarity, measures how features differ regarding associations within spatial zones and associations among the whole study area (Goodchild, M.F. 2004; Zhang et al., 2022). The characteristic of SSH and factors' interactions can be measured by geographical detector (GD), which is a statistical measure by discretizing factors (Wang et al., 2022; Zhang et al., 2024b). The method of GD and the feature of SSH have the potential to be integrated into GNNs to show spatial heterogeneity. Significant differences in variables across the space may be caused by the variance of spatial dependence level from place to place, and GD-based methods can capture this phenomenon (Zhang et al., 2024a).

On the other hand, the trial of integrating GD into GNN by showing a discrete change of heterogeneity among geographical neighbors into a graph structure may fit the SST framework and improve the spatial model. Estimation error in spatial statistics originates from three interconnected components (Wang et al., 2020). First, population characteristics include the overall spatial attributes of the study area, such as spatial autocorrelation (SAC), spatial heterogeneity, and global and local spatial patterns (Fischer and Wang, 2011; Wang et al., 2020), we quantify SSH in the response variable Y using GD, while preserving SAC through graph nodes and edges that enforce spatial connectivity and feature-based autocorrelation. Second, sample conditions involve data selection, representativeness, quality, and spatial distribution (Kent et al., 2006). Our training data covers all strata of Y, avoiding stratified sampling, and oversampling for rare categories shall be employed to prevent class imbalance. Third, estimation method characteristics pertain to the properties of the statistical methods used, including their assumptions, model structures, and handling of spatial dependencies (Li et al., 2015), we dynamically adjust neighbor influences (spatial interactions) via feature similarity between adjacent spatial units facing mixed SAC-SSH regimes, where neighbors within the same feature stratum exert more substantial impact, it is stratified-like estimation.

Thus, this research presents the Geographically Informed Graph Neural Networks (GIGNN) as a variant of the GNNs method, further considering spatial relations on connectivity. Besides working as a method for factor selection, the GD-based method is also applied to demonstrate differences among geographic neighbours by spatial zones when setting GNNs. We prove that GIGNN, with updates on further integration with spatial concepts, has better model performance in supporting intelligent urban decision-making. The rest of the article is organized as follows: Section 2 demonstrates the concept and design of GIGNN, followed by a simulation experiment in Section 3 and a case study of urbanization factor analysis in Western Australia in Section 4. Section 5 shows the model results and comparison, and a further discussion is arranged in Section 6.

2. Geographically informed graph neural networks

2.1. Design principles

The GIGNN framework integrates geospatial principles with adaptive graph learning to model non-stationary spatial interactions. Grounded in the SST framework (Wang et al., 2020) and the laws of geography (Tobler et al., 2004; Miller et al., 2004), it addresses two inherent properties of spatial systems: attribute correlations decay with topological distance but may persist across distant regions sharing similar features; abrupt spatial heterogeneity occurs when adjacent units exhibit significant feature divergence. These principles guide the model's architecture, which operates on predefined spatial units stratified by features such as urbanization levels. Instead of static spatial weight matrices, GIGNN employs feature-sensitive graph convolutions to dynamically adjust neighbor impacts on itself. This process mimics heterogeneous kernel density estimation, where edge weights are determined by both topological proximity and feature similarity. Physically adjacent nodes with dissimilar features receive suppressed weights to reflect spatial heterogeneity, while higher-order neighbors with matching attributes retain weak connections to capture long-range dependencies. Such dual adaptation resolves edge effects at stratum boundaries and enables selective information propagation across heterogeneous regions. The framework thus unifies distance-decay patterns, feature-mediated correlations, and discontinuity handling within a single optimization process, making it well-suited for simulating complex spatial interactions in diverse geographical phenomena.

2.2. Architecture of GIGNN

GIGNN's architecture consists of a geographically informed process and a GNN framework. This integration is designed to

capitalize on the strengths of additional spatial features and GNNs to improve spatial prediction accuracy and elucidate local variable influences within spatial scenarios.

2.2.1. Geographically informed process

The initial phase of GIGNN involves spatial influence hypotheses, which are validated using spatial or statistical measures to identify significant factors influencing the dependent variable (Miller et al., 2007; Wang et al., 2022). Unlike using a single factor detector for attribute selection, we apply the interaction detector using geographical detector methods. Given the architecture of GNN, factors with more strength on interactive forces when determining the dependent variable can be more capable of spatial prediction than others.

2.2.2. Graph construction

In the GIGNN model, we also consider additional spatial characteristics that some adjacent spatial neighbors can be very different, as shown in the featured attributes, and this feature is quantified by spatial stratified heterogeneity before training GNNs. Geographically informed processes are translated into a graph-based representation using a graph $G = (N, E)$. The set N represents geographic entities, such as regions or locations, with each node embedded with spatially discretized feature values derived from initial analysis. These attributes are re-quantified and stratified using the GD (Wang et al., 2022), a statistical tool designed to

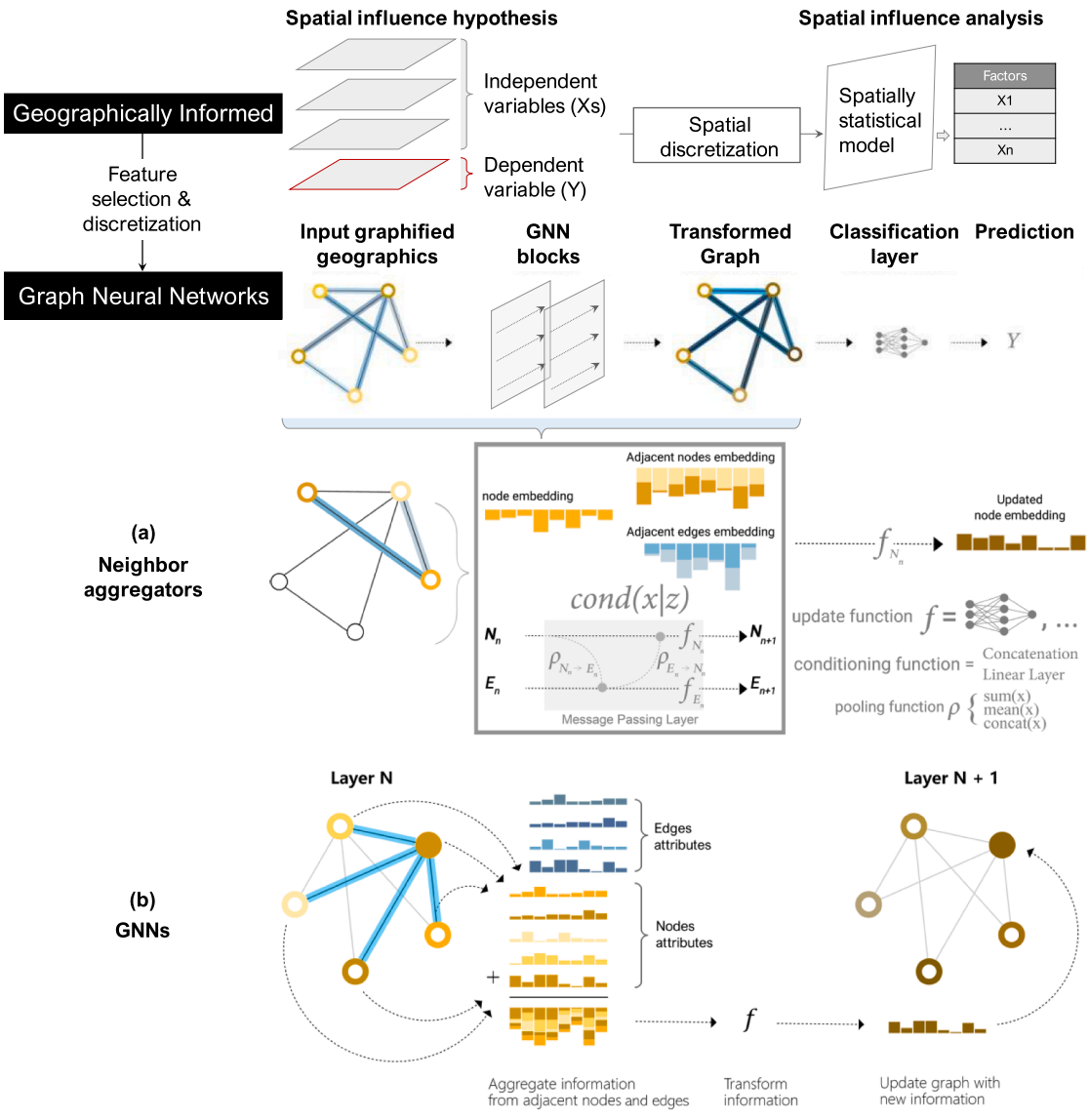

Fig. 1. Architecture of GIGNN for spatial modelling. *Note: Inspired by Sanchez-Lengeling et al. (2021).*

determine the explanatory power of various factors influencing the dependent variable and to discretize continuous variables by spatial zones (1). The set E denotes spatial interactions between adjacent nodes. The attributes on edges are determined by the feature differences between two nodes, using a Gaussian Kernel function (2) to reflect homogeneity and heterogeneity (Burke et al., 2021).

$$\boldsymbol{Q} = 1 - \frac{\sum_{h=1}^{L} \boldsymbol{n_h \sigma_h^2}}{\boldsymbol{N \sigma^2}} \tag{1}$$

where Q measures the explanatory power of a variable, L is the number of strata that are classified by Jenks natural break method, n_h is the count in each stratum, σ_h^2 is the stratum variance, N is the total observations, and σ^2 is the overall variance.

$$K(x_i, x_j) = \exp\left(- \frac{\| x_i - x_j \|^2}{2\sigma^2} \right) \tag{2}$$

where $K(x_i, x_j)$ represents the Gaussian Kernel function between node i and node j, with x_i and x_j being their respective feature vectors. The term $\| x_i - x_j \|^2$ denotes the Euclidean distance squared between the feature vectors, and $\sigma = 2$ is a predefined parameter controlling the spread of the kernel.

GeoDetector (GD), as a measure of spatial stratified heterogeneity, is also applied to categorize spatial zones for selected variables and re-quantify continuous variables to highlight and signify features' differences among geographical neighbors. Continuous variable values for spatial units are re-quantified according to statistical levels quantified by GD. For each continuous variable, spatial units are relabeled according to the ascending order of their group-level overall statistic, with labels ranging from 1 (assigned to units in the group with the minimum statistic) to n (for those in the group with the maximum statistic). This relabeling and re-quantification process will signify spatial neighbors' differences in features. Then, the Gaussian Kernel function is applied to measure the distance between nodes according to the new feature vector.

2.2.3. Graph neural network processing

The GIGNN model, grounded in the GraphSAGE architecture (Ding et al., 2021; Hamilton et al., 2017), as shown in Fig. 1, benefits from the message-passing operation to handle geographical entities' attributes and spatial effects. It integrates the Neighbor Aggregator (NA) module and Graph Convolutional Network (GCN) Layer components into a comprehensive system for spatial data processing. The NA module captures the local spatial structure and context by aggregating information from k-order neighbors (4), which aligns with the laws of geography that emphasize the importance of spatial proximity and interaction. The GCN Layer integrates and transforms node features by combining the aggregated features from neighbors with the node's features (5), further enhancing the model's ability to capture spatial heterogeneity. The forward propagation process sequentially employs GCN layers to update node features by aggregating and transforming the information within the graph structure. This design allows GIGNN to effectively simulate spatial interactions and heterogeneity, following both the SST framework and the laws of geography.

$$H^{(L)} = \text{GIGNN}\left(H^{(0)}, G\right) \tag{3}$$

where $H^{(0)}$ is the initial node features matrix, G is the graph, and $H^{(L)}$ is the output node features matrix after L layers of graph convolution. The final output is then passed through a classifier for node classification or other downstream tasks.

$$h_v^{(l+1)} = \sigma\left(W^{(l)} \cdot \mathrm{A}_k \left(\left\{ h_u^{(l)} : u \in N_k(v) \right\} \right) + b^{(l)} \right) \tag{4}$$

where: $h_v^{(l+1)}$ is the updated feature vector of node v at layer $l+1$. $N_k(v)$ represents the set of k-order neighbors of node v. $h_u^{(l)}$ is the feature vector of a k-order neighbor u of node v at layer l. $\mathrm{A_k}$ is the aggregation function (sum, mean, concat) applied to the features of k-order neighbors. $W^{(l)}$ and $b^{(l)}$ are the weight matrix and bias vector for layer l, respectively. σ is a non-linear activation function.

$$h_v^{(l+1)} = \text{ACT}\left(\mathrm{A}\left(\left\{ h_u^{(l)} : u \in N(v) \right\} \right), h_v^{(l)} \right) \tag{5}$$

where $h_v^{(l+1)}$ is the updated feature vector of node v at layer $l+1, h_v^{(l)}$ is the feature vector of node v at layer l, and ACT is an activation function. The A is the aggregation function (sum, mean, concat) used to combine the features of node v and its neighbors, and $N(v)$ to produce a new feature representation

3. Spatial data simulation experiment

3.1. Scenarios

A synthetic dataset was generated with explicit spatial dependency and heterogeneity to evaluate the performance of GIGNN. The simulation framework was designed as follows:

A 10×10 hexagonal lattice grid scenario containing 100 regularly spaced spatial units was constructed. Adjacency between units was defined by the Queen contiguity rule, where two hexagons sharing a common edge or vertex were considered neighbors.

Spatially autocorrelated explanatory variables X_k ($k = 1,2,\ldots,\mathrm{K}$) were generated through an iterative spatial autoregressive process

(6), followed by min-max normalization (7). This procedure ensured spatial dependency with Moran's I greater than 0.8.

$$X_k^{(t+1)} = 10 \cdot X_k^{(t)} + 0.8 \cdot \sum_{j=1}^{n} w_{ij} X_k^{(t)}(j), \tag{6}$$

$$X_k = \frac{X_k - \min(X_k)}{\max(X_k) - \min(X_k)}. \tag{7}$$

The response variable Y was formulated as a linear combination of the explanatory variables X_k with fixed regression coefficients β_k sampled from a uniform distribution (8). The spatially autocorrelated error term was generated through a spatial filtering process with Gaussian white noise (9).

$$Y = \sum_{k=1}^{K} \beta_k X_k + \epsilon, \tag{8}$$

where regression coefficients β_k are fixed values sampled from $\beta_k \sim \mathscr{U}(0.4, 0.8)$. The spatially autocorrelated error term ϵ is generated through a spatial filtering process:

$$\epsilon^{(t+1)} = 0.5 \cdot \epsilon^{(t)} + 0.6 \cdot \sum_{j=1}^{n} w_{ij} \epsilon^{(t)}(j) + \eta, \tag{9}$$

with $\eta \sim \mathscr{N}(0, 0.05^2)$ representing Gaussian white noise.

The study area was partitioned into four disjoint regions using k-means clustering based on hexagon centroids. Region-specific variations were introduced to simulate localized spatial effects by scaling the error term within each cluster. The dataset was generated following a spatial scenario of global spatial autocorrelation with heterogeneity in some local areas.

3.2. Experiment

The synthetic dataset was designed to show both global spatial autocorrelation of variables and local heterogeneity of the different effects of Xs on Y within various zones (Fig. 2). GD was employed to detect spatial factors and interactions to evaluate the performance of GIGNN in capturing these spatial characteristics.

As shown in Table 1, the independent variables $x1$, $x2$, and $x3$ exhibit significant influences on dependent variable Y, with $x1$ having the highest spatial explanatory power. Interaction detection reveals that the combined effect of $x1$ and $x3$ has the strongest spatial interaction. This indicates that the GD effectively captures the spatial dependency among the variables. GIGNN is expected to model this complex spatial relationship accurately based on correct explainable spatial hypotheses and stratification of spatial features.

To evaluate GIGNN's predictive performance, diagnostic metrics were calculated for both training and testing subsets. As shown in Table 2, the training subset achieved an accuracy of 0.969, demonstrating GIGNN's ability to learn spatial patterns effectively. For the testing subset, the F1 score, precision, and recall were 0.783, 0.825, and 0.789, respectively, indicating a balanced performance and accurate prediction of the response variable despite spatial heterogeneity and autocorrelation.

In summary, GIGNN demonstrated the ability to capture spatial dependency and features' heterogeneity in the synthetic dataset. High training accuracy and balanced testing metrics indicated effective spatial pattern modeling and accurate predictions. The random spatial distribution of prediction bias further confirmed GIGNN's robustness in handling complex spatial dependencies.

4. Case study - urbanization factor analysis of Western Australia

This research applies GIGNN to a case study to demonstrate how this new GeoAI method can help support decision-making in human geography and broader fields. In this study, we used GIGNN to investigate the urbanization level of the Greater Perth Area and its associated factor analysis, considering Perth's unneglected socio-economic role statewide and nationwide.

Perth is the capital city of Western Australia (WA) and the fourth largest city in Australia in terms of population. According to the national census, WA has a population of over 2.5 million, around 11 % of the national population (Australian Bureau of Statistics,

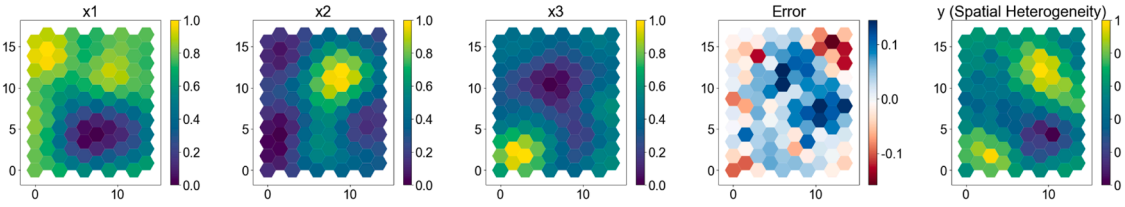

Fig. 2. Map of simulation dataset for assessing GIGNN modelling.

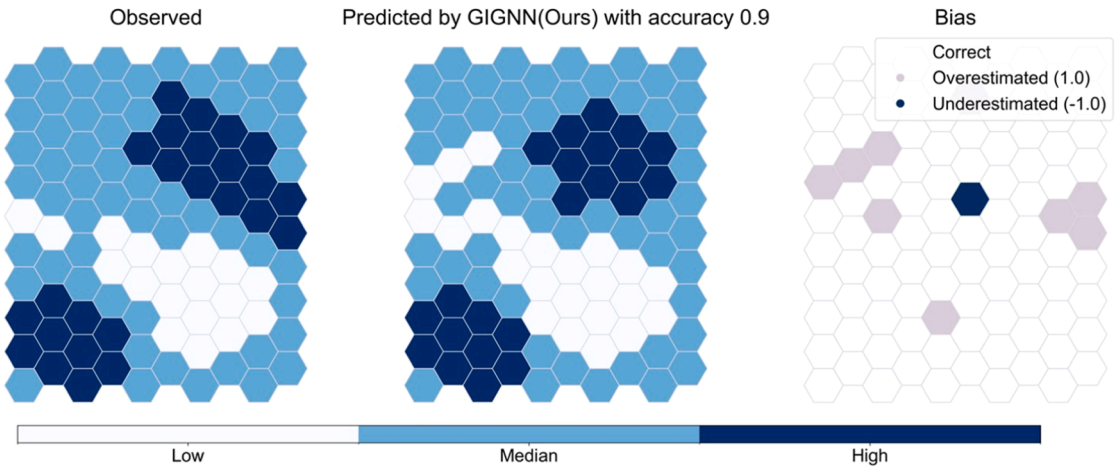

Fig. 3. Comparison between the observed and the predicted by GIGNN.

Table 1
Results of simulation data analysis using GD.

Factor detection		Interaction detection		
Variable	*Q*	Factor A	Factor B	*Q* for interaction
x1	0.383*	x1	x3	0.748*
x3	0.309*	x2	x3	0.585*
x2	0.191*	x1	x2	0.547*

*Note: * indicates significance at the 0.01 level.*

Table 2
Diagnostic metrics for training and testing.

Subset	Metrics	Global	High	Low	Median
Training	Accuracy	0.969	0.968	0.97	0.969
Testing	F1	0.783	0.667	0.857	0.783
	Precession	0.825	0.600	0.833	0.857
	Recall	0.789	0.75	1	0.750

Notes: Global metrics are calculated using weighted average.

The spatial distribution of prediction bias was further examined to determine if there were spatial clusters of residuals. Fig. 3 compares observed and predicted values by GIGNN, with an accuracy of 0.9. The Moran's I value of the bias is 0.111, with a Z-score of 0.657 and a p-value of 0.302, indicating a random spatial distribution pattern. This suggested that GIGNN did not systematically overestimate or underestimate the response variable in any specific spatial region, which is consistent with the dataset's design. GIGNN effectively modeled complex spatial dependencies and produced unbiased predictions across the study area.

2023c). WA also provides a significant economic contribution and employment to the nation, with 12.6 % of the total wages and salaries, 16 % of sales and service income, and 11 % of full employment (Australian Bureau of Statistics, 2023a). The Greater Perth Area has around 80 % of the WA population, which is the core of WA. Furthermore, the Greater Perth Area has had steady annual population growth and urbanization development over the decades (Australian Bureau of Statistics, 2023c). Thus, investigating the urbanization level and its associated factor analysis could help policymakers and research experts understand how human activity factors are associated with the greater urbanization area and provide insights for intelligent decision-making for urbanization and socio-economic benefits.

4.1. Data

4.1.1. Independent variables

In this study, we selected candidate independent variables from the Australian national census data. The Australian Bureau of Statistics (ABS) conducts a federal census every five years, covering various socioeconomic information for residents and communities. From the perspective of individuals, the census data collects detailed information on residents, including but not limited to occupation, salary, income level, transport preference, education level, and family structures. From the aspect of surveys on communities, ABS integrated the national census data and concluded further information, such as income distribution and socio-economic development

index, on the local community performance (Australian Bureau of Statistics, 2023d).

Statistical Area Level 2 (SA2) is a medium-sized spatial boundary proposed by ABS. The Australian continent can be divided into around 2500 non-overlapping SA2 areas, and each SA2 area generally has a population of 3000 to 25,000. The SA2 spatial boundaries can reflect social and economic interaction among communities by considering functional areas, suburban and locality structures, and local government structures (Australian Bureau of Statistics, 2021). Furthermore, SA2 is also the finest ABS-defined spatial boundaries, compatible with datasets within the 'Data by Region Methodology,' which includes various aspects of socio-economic survey information from economy and industry to family and community (Australian Bureau of Statistics, 2023b). Thus, in this research, we investigated how human activity factors are associated with the urbanization level at the SA2 level and provided model computation at this finest possible spatial scale.

Fig. 4 shows the spatial boundaries of SA2 areas in the Greater Perth Area and the statistical distribution of a dozen candidate factors associated with the urbanization level, summarized at the SA2 level. These datasets representing features of each SA2 area can be categorized into 'economy,' 'education,' 'employment,' 'family and household structure,' and 'transport.' This information was accessed from ABS and integrated by GIS. Further details of the census data are summarized in Table 3.

4.1.2. Dependent variable

To assess the urbanization levels of Statistical Area Level 2 (SA2) regions in Perth for 2016, the Average Nighttime Light Index (ANLI) was employed. ANLI indicates urbanization, economic activity, and energy consumption, derived from remotely sensed nighttime light data. This index provides a normalized measure of nighttime brightness, facilitating comparative analysis of urbanization levels across different SA2 regions. The intensity of artificial lighting, as quantified by ANLI, reflects the extent of urban development and offers insights into the spatial distribution of urban areas within Perth in 2016 (Fig. 5). The ANLI was computed using the following formula:

$$ANLI = \frac{\sum_{i=1}^{n} L_i}{A} \tag{10}$$

where L_i represents the luminance value of each pixel within the specified SA2 region, n is the total number of pixels in the region, and A denotes the total area of the region in square kilometers. The luminance values were extracted from the VIIRS Day/Night Band nighttime light data set (https://eogdata.mines.edu/products/vnl/), a satellite imagery source known for its high resolution and accuracy in reflecting the intensity of ground lighting.

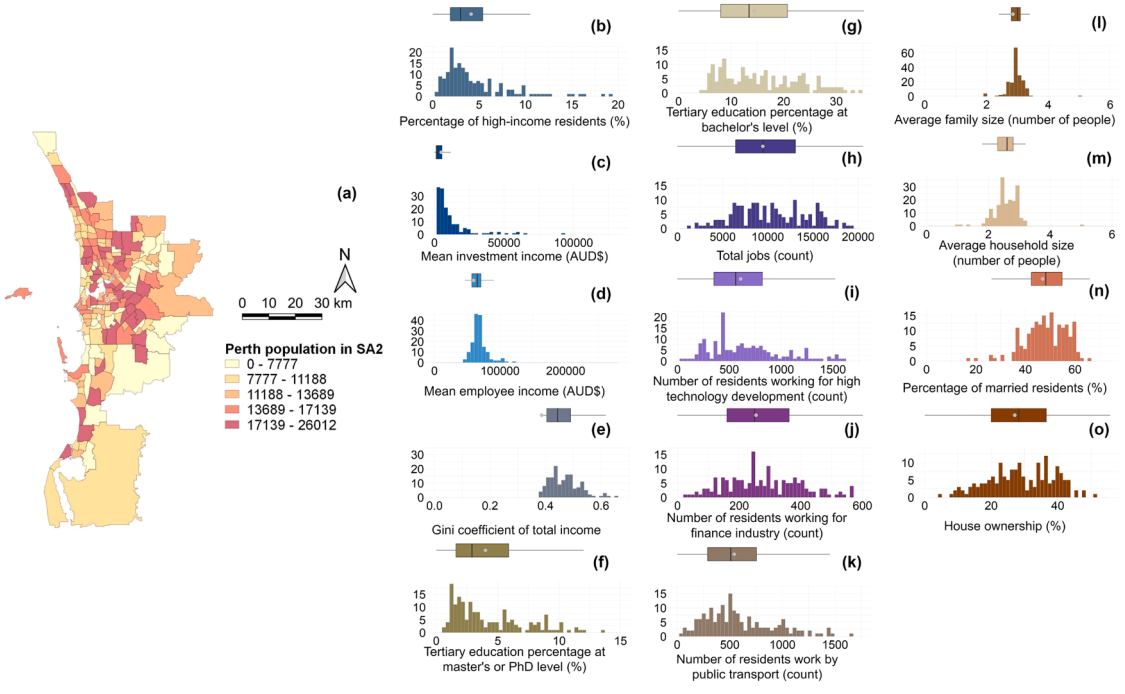

Fig. 4. Statistical Area Level 2 (SA2) and data distribution. (a). SA2 spatial boundaries and population in the Greater Perth Area. Statistical distribution of factors at SA2 level, (b). Percentage of high-income residents, (c). Mean investment income, (d). Mean employee income, (e). Gini coefficient of total income, (f). Tertiary education percentage at postgraduate level, (g). Tertiary education percentage at bachelor's level, (h). Total jobs, (i). Number of residents working for high technology development, (j). Number of residents working in the financial industry, (k). Number of residents work by public transport, (l). Average family size, (m). Average household size, (n). Percentage of married residents, (o). House ownership.

Table 3
Candidate influential factors from census data summary.

Independent factor censused at SA2	Data name shown in the national census	Unit	Factor category
Percentage of high-income residents	$3000 or more per week	%	Economy
Mean investment income	Mean investment income	AUD$	Economy
Mean employee income	Mean employee income	AUD$	Economy
Gini coefficient of total income	Total income (excluding government pensions and allowances) – Gini coefficient	–	Economy
Tertiary education percentage at bachelor's level	Bachelor's degree	%	Education
Tertiary education percentage at master's or PhD level	Postgraduate degree	%	Education
Total jobs	Number of jobs	Count	Employment
Number of residents working for high technology development	Number of employee jobs - professional, scientific, and technical services	Count	Employment
Number of residents working in the finance industry	Number of employee jobs - finance and insurance services	Count	Employment
Average family size	Average family size	Number of people	Family and household
Average household size	Average household size	Number of people	Family and household
Percentage of married residents	Married	%	Family and household
House ownership	Owned Outright	%	Family and household
Number of residents work by public transport	Used at least one form of public transport	Count	Transport

4.2. Methodology

This study presents the GIGNN model's architecture (Fig. 6) and research workflow (Fig. 7). The research framework consists of four steps and provides the model for urbanization analysis in the Great Perth Area.

The first step is dataset construction. Data processing at the SA2 level forms the foundational spatial dataset. According to the topological relationship, the geometric structure of the spatial dataset was transformed into a graph structure.

The second step is factor selection and quantification. GD (for target group) or Spearman's rank correlation (for other groups) identified factors significantly correlated with urbanization levels in 2016. The target group included the top three key factors from the interaction detection network with high centrality degree and Q value, integrating spatially discerned factors from SSH spatial zones as node feature inputs. The control and benchmark groups used all significant relevant factors with raw value as features. For GNN models, edge features were calculated using the Gaussian kernel function based on characteristics of connected node pairs.

The third step is model grouping. Three modeling groups were established for comparative analysis. The target group used the GIGNN model. The control group included GNNs such as GAT, GIN, ChebNet, and MPNN. The benchmark group used a machine learning model, Random Forest.

The fourth step is performance comparison. During the modeling stage, the models were evaluated using k-fold cross-validation for training and testing. Additionally, their simulation and prediction performances were validated. The performance metrics used to assess model efficacy included accuracy, F1 score, precision, and recall. A generalized spatial prediction for 2021 was conducted to ensure spatial accuracy and reliability.

5. Results

5.1. Factor selection

Interaction detection using the GD method identified factor pairs with q-values exceeding the maximum single-factor threshold, indicating that the urbanization level is influenced by the nonlinear enhancement of multiple strong interacting educational-economic feedback, housing market stratification, and household-driven demographic pressures, providing theoretical grounding for target group (GIGNN model) internal learning patterns in urbanization levels.

In the interaction network analysis depicted in Fig. 8, three central features marked with "★" were prioritized: tertiary education at the master's level, house ownership, and average family size. These features encapsulate the nonlinear enhancement among education hierarchies, housing accessibility, and demographic constraints. Following factor selection, the factors (Xs) were categorized into five groups, coded from 1 to 5. The urbanization level (Y) was divided into three groups, coded from 1 to 3.

5.2. Modelling

5.2.1. Performances on training sets

Model performance was assessed using k-fold cross-validation with five rounds and 1000 epochs for each round. This method evaluated training stability and predictive accuracy across three levels of urbanization. The results provide insights into the model's

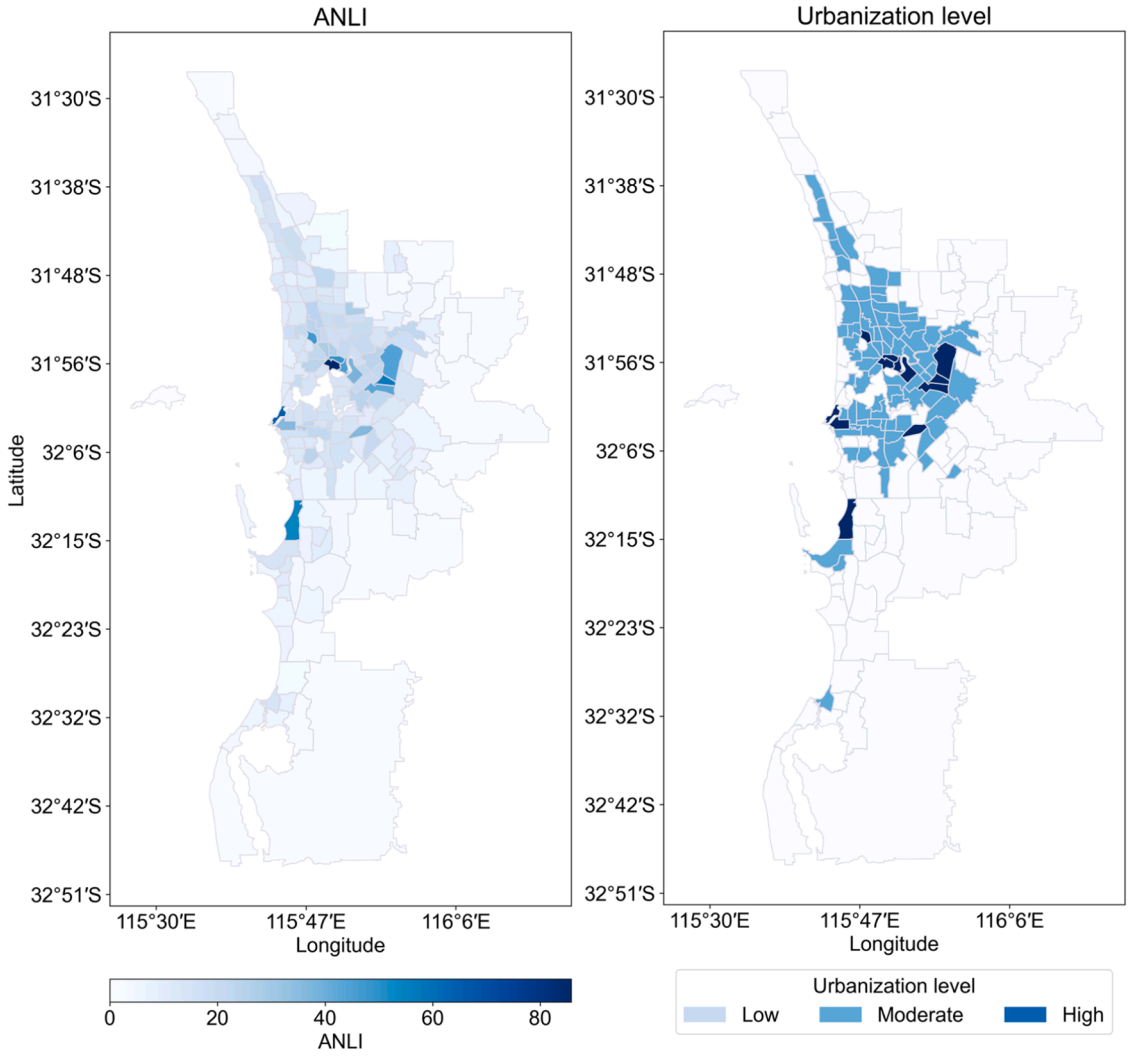

Fig. 5. Map of urbanization level measured by ANLI in Perth (2016).

capabilities in classifying diverse urban contexts (Fig. 9).

GIGNN demonstrated superior performance, achieving the highest global accuracy of 0.957 and consistently dominating across all urbanization levels. Its F1-score in low urbanization areas reached 0.974, indicating high precision in classifying less developed regions. Even in high urbanization areas, GIGNN maintained a robust F1-score of 0.923. ChebNet ranked second with a global accuracy of 0.776 and F1-scores ranging from 0.728 to 0.812 across different urbanization levels. ChebNet exhibited a 15.7 % accuracy gap when compared to GIGNN, particularly in high urbanization areas where GIGNN's F1-score was 0.625 higher than that of ChebNet's.

Other models demonstrated less consistent performance. RF achieved a global accuracy of 0.533, showing some competence but facing significant challenges in highly urbanized areas (F1-score: 0.333). GAT and GIN displayed considerable fluctuations in F1-scores across different levels of urbanization, with accuracies of 0.566 and 0.493, respectively. MPNN recorded the weakest overall performance with a global accuracy of 0.48.

Overall, GIGNN surpassed other models in accuracy and stability. Its lowest F1 Score in highly urbanized areas (0.923) was higher than the best scores of most competitors, emphasizing its robustness and suitability for urbanization-level prediction tasks.

5.2.2. Performances on test sets

The k-fold cross-validation results demonstrate the superior performance of the GIGNN model across various levels of urbanization (Table 4). GIGNN surpassed the benchmark RF model and control groups (GAT, GIN, ChebNet, MPNN) with global metrics of F1 = 0.644, precision = 0.696, and recall = 0.649. This superiority is attributed to its hybrid architecture, which combines hierarchical graph pooling and adaptive attention mechanisms, effectively preserving multi-scale spatial features and mitigating overfitting.

In contrast, the benchmark RF model has limitations in modeling spatial dependencies, resulting in lower precision (0.557) and insufficient discrimination of urbanization levels. Control models exhibited category-specific deficiencies: GAT and GIN struggled with

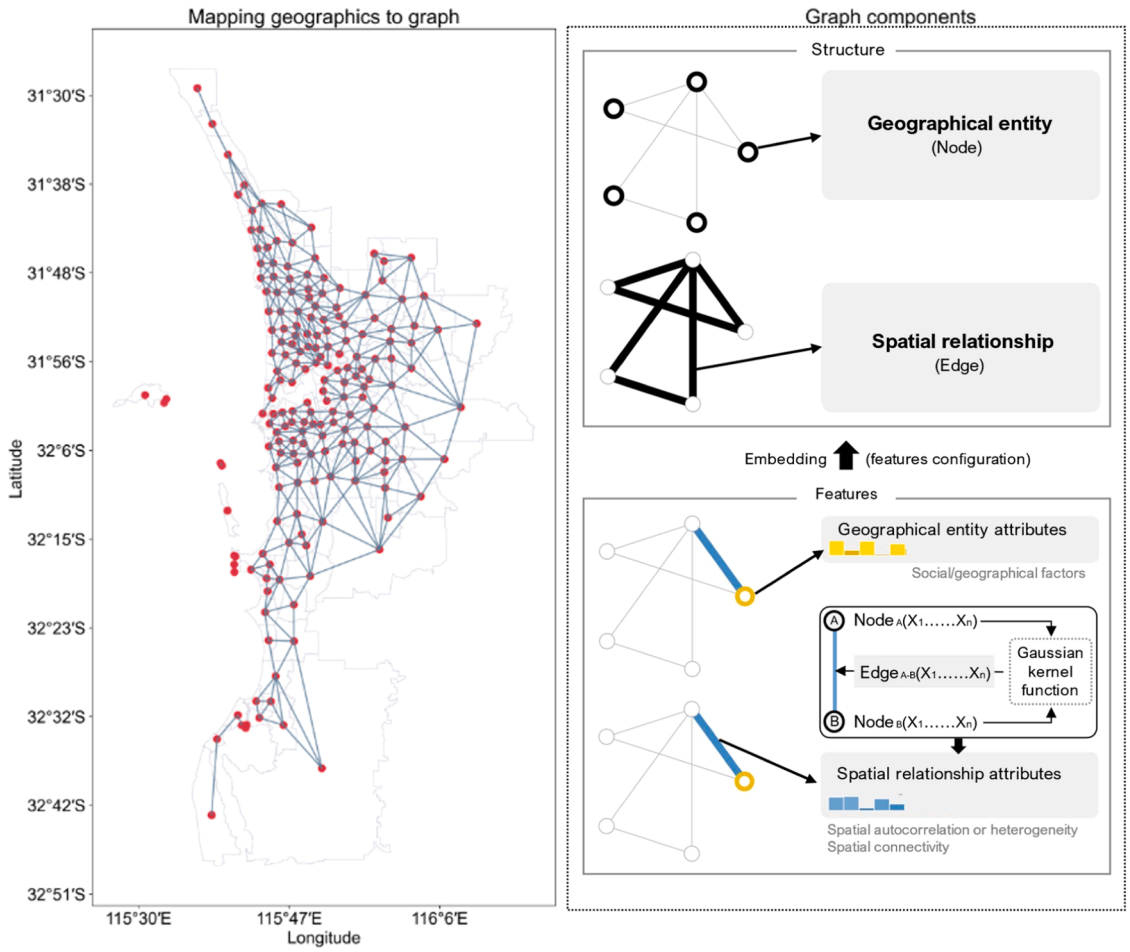

Fig. 6. The procedure for GIGNN structural and feature configuration.

high urbanization predictions due to fixed aggregation mechanisms, while ChebNet displayed a spectral bias with a recall-precision trade-off. MPNN's instability in heterogeneous urban graphs leads to a significant performance drop. GIGNN was globally preferred for comprehensive urbanization analysis, while control models may offer niche applications, such as ChebNet for low-urbanization recall or GAT for moderate urbanization detection.

5.3. Spatial simulation and model training for the year 2016

The GIGNN model was assessed for its performance in simulating urbanization levels within the study area for 2016, achieving an accuracy of 84.1 % (Fig. 10). Bias analysis was conducted by comparing prediction and observation codes, which revealed that 155 areas were correctly identified among the simulated results, 25 regions were overestimated, and 9 areas were underestimated (including 7 instances of minor underestimation and 2 instances of major underestimation). This pattern indicated a potential bias in the model towards overestimating urbanization levels.

Fig. 11

Validation results highlighted challenges in distinguishing transitions between urbanization levels (Table 5). Performance metrics revealed reduced recall for median urbanization and lower precision for high urbanization, indicating difficulties in accurately classifying intermediate and high-level urban development. Spatial autocorrelation analysis (Moran's $I = 0.089$, $p = 0.282$) confirmed no significant spatial clustering in residuals, suggesting that the model's errors were random distributed.

The GIGNN model successfully addressed the heterogeneity in the spatial distribution of urbanization levels and the imbalanced statistical distribution of data across categories. This emphasized its capability for urban spatial analysis in 2016, although targeted refinements are still needed to enhance classification consistency, particularly for transitional and high-density urban areas zones.

5.4. Spatial prediction for the year 2021 using trained models from 2016

The GIGNN model, trained on 2016 geospatial data, demonstrated strong performance when applied to 2021 urbanization

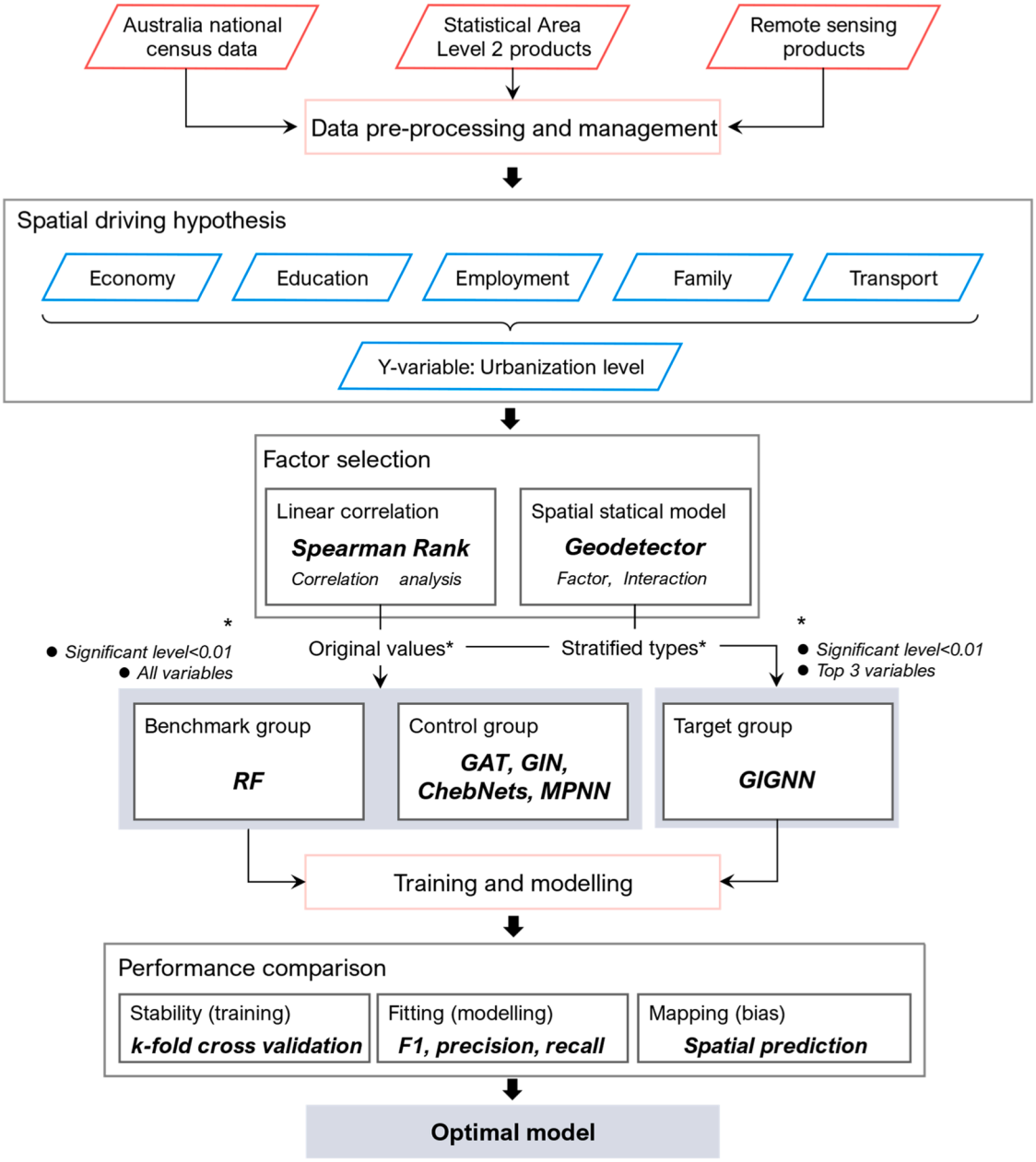

Fig. 7. Workflow of case study for finding optimal model.

predictions. Comparative evaluations against RF were performed, as other graph-based models (GAT, GIN, ChebNet, MPNN) showed poor performance in preliminary tests.

Quantitatively, GIGNN achieved impressive temporal adaptability, with an accuracy of 81.0 %, significantly outperforming RF (65.6 %) by 15.4 %, confirming its ability to retain learned spatiotemporal patterns. Error distribution analysis indicated that GIGNN correctly classified 153 spatial units with minimal overestimation and controlled underestimation. In contrast, RF displayed systematic biases, particularly in transitional zones where 68 % of errors clustered, reflecting its inability to model urban evolution structurally. Spatial autocorrelation diagnostics further distinguished the two approaches. GIGNN's residuals showed no significant spatial clustering (Moran's $I = 0.014$, $p = 0.309$), confirming effective learning of spatial dependency. Conversely, RF's errors exhibited strong autocorrelation (Moran's $I = 0.208$, $p = 0.003$), revealing a lack of spatial pattern learning, especially in low-to-moderate urbanization cross areas where overlapping features challenged non-structural models.

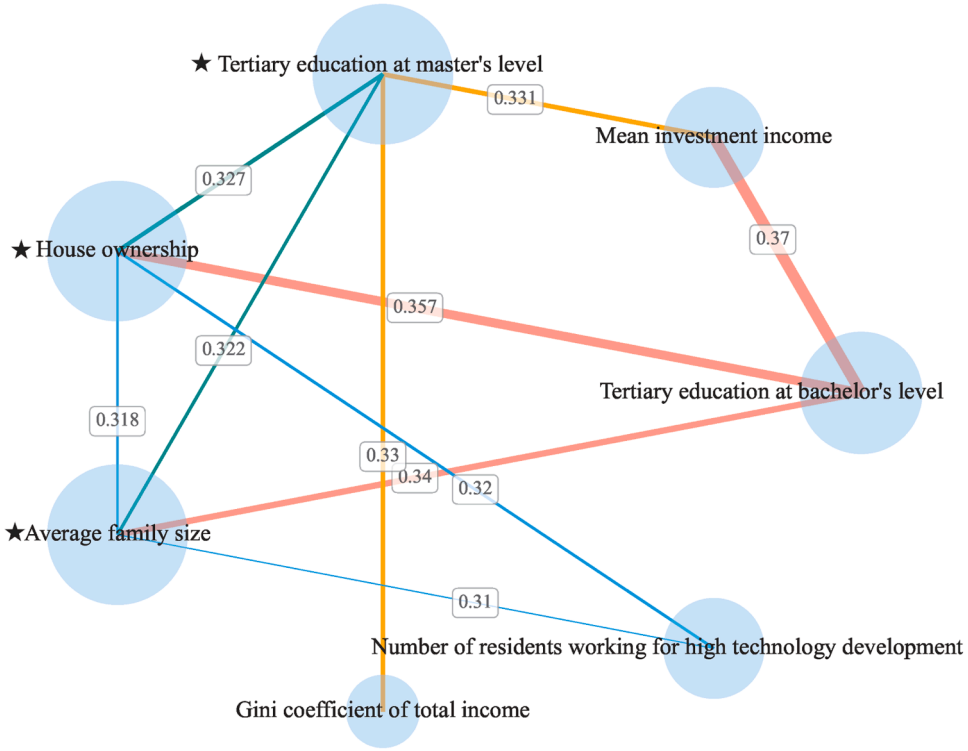

Fig. 8. The interaction network was generated by the top 10 interaction results of GD.

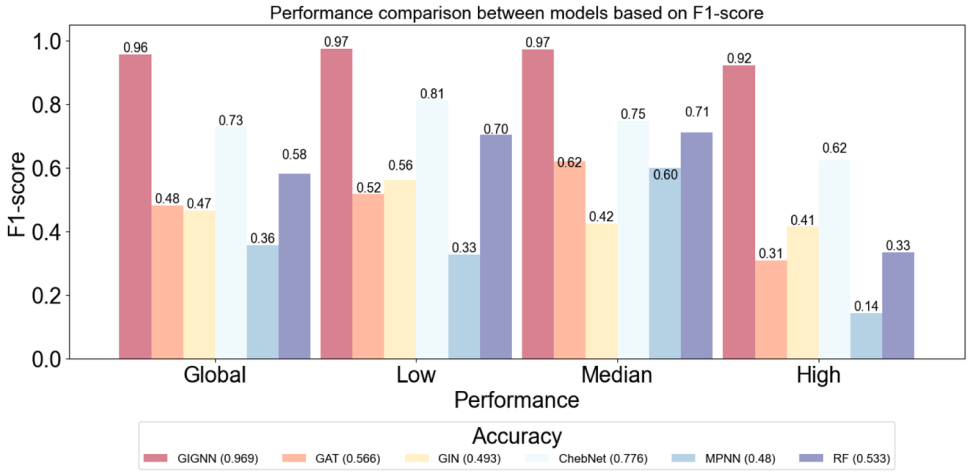

Fig. 9. Performance comparison at training sets.

6. Discussions

6.1. Inspirations from simulation tests and case studies

Simulation tests and case studies indicate that our model performs better in scenarios with significant spatial interactions. It can capture complex spatial cases involving multiple independent variables and their spatial interactions with the dependent variable. While spatial attribution analysis can quantify spatial stratified heterogeneity to assess the explanatory power of factors shaping the spatial patterns of observed objects, our model incorporates these driving mechanisms into the internal operations of GNNs to enhance spatial relational modeling. This approach allows for a more nuanced understanding of spatial patterns and improves spatial modeling performance.

Table 4
Comparison of median performance metrics across models at test sets using K-fold cross-validation.

Metrics	Classification	GIGNN	GAT	GIN	ChebNet	MPNN	RF	Best model
F1	Global	**0.644**	0.577	0.438	0.496	0.369	0.553	GIGNN
	High urbanization	**0.400**	0	0	0	0	0	GIGNN
	Low urbanization	**0.718**	0.667	0.514	0.615	0.524	0.667	GIGNN
	Median urbanization	**0.600**	0.600	0.438	0.485	0.286	0.545	GIGNN
Precision	Global	**0.696**	0.622	0.446	0.553	0.418	0.557	GIGNN
	High urbanization	**0.286**	0	0	0	0	0	GIGNN
	Low urbanization	**0.765**	0.588	0.500	0.609	0.459	0.625	GIGNN
	Median urbanization	**0.619**	0.571	0.444	0.474	0.321	0.6	GIGNN
Recall	Global	**0.649**	0.595	0.459	0.541	0.459	0.579	GIGNN
	High urbanization	**0.500**	0	0	0	0	0	GIGNN
	Low urbanization	0.696	0.609	0.522	**0.706**	0.600	0.650	ChebNet
	Median urbanization	0.615	**0.632**	0.444	0.526	0.308	0.500	GAT

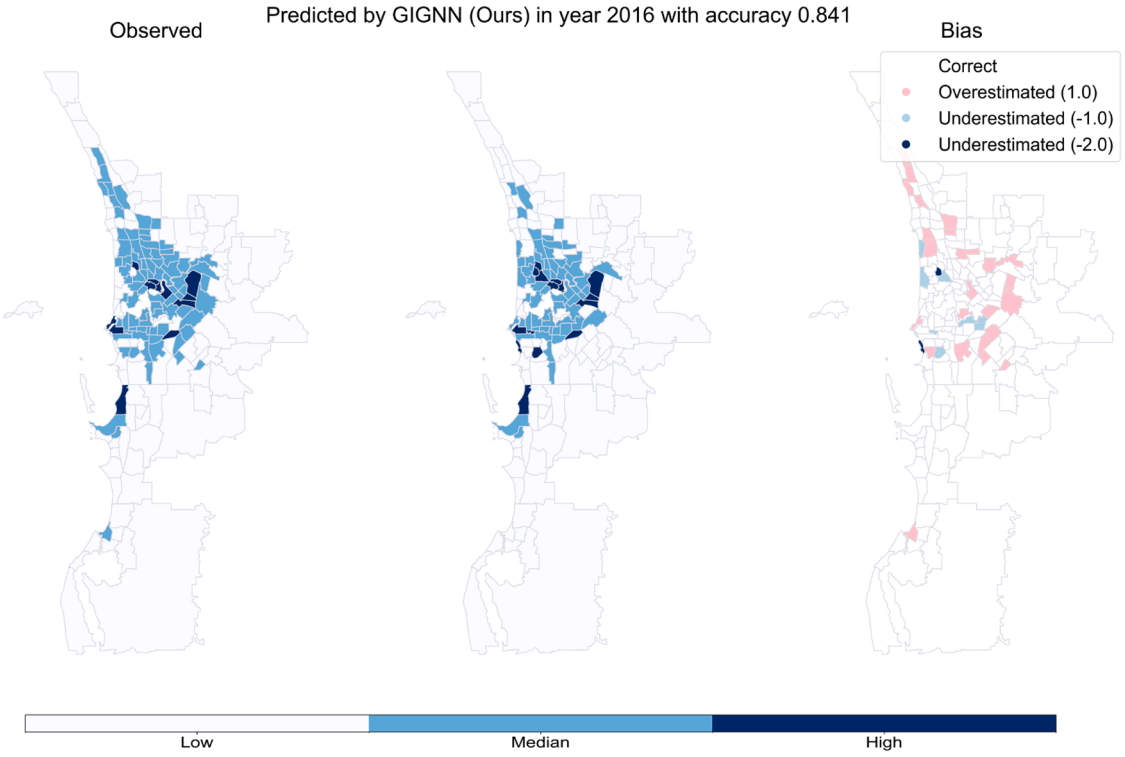

Fig. 10. Comparison between observations and predictions. *Notes: The levels of urbanization were encoded as numeric categories, ranging from low to high. The bias refers to the difference in numeric coding between the predicted and observed categories. A bias of 0 indicates that the predicted category matches the observed category exactly. A positive value signifies that the model overestimated the urbanization level by n categories in the current region, and* vice versa.

Specifically, spatial discretization enables the convergence of variables into distinct partitions, thereby enhancing the local feature representation of spatial units. Meanwhile, the graph structure quantitatively characterizes spatial homogeneity and heterogeneity across multiple features. First, each spatial unit holds its features and integrates the similarities and differences between its own and neighboring features, broadening the scope of spatial attributes. Second, between graph convolution layers, the attribute updates of each spatial unit are influenced by its k-order neighbors, simulating the mechanism of spatial influence decay not only by distance but also by features. Within the local range of a spatial unit, its feature updates are constrained by the feature differences among neighbors: if the difference in a particular feature between two spatial units is significant, the increment of that feature will be limited; if the features are similar, the increment will be more pronounced. Finally, while the graph's structure remains unchanged after graph convolution processing, this process simulates the spatial interactions between features and considers spatial effects. Therefore, when the updated high-dimensional attribute vectors of each spatial unit are mapped to the classification of observed objects, they can retain their spatial distribution characteristics and address the challenges of imbalanced categories among observed objects.

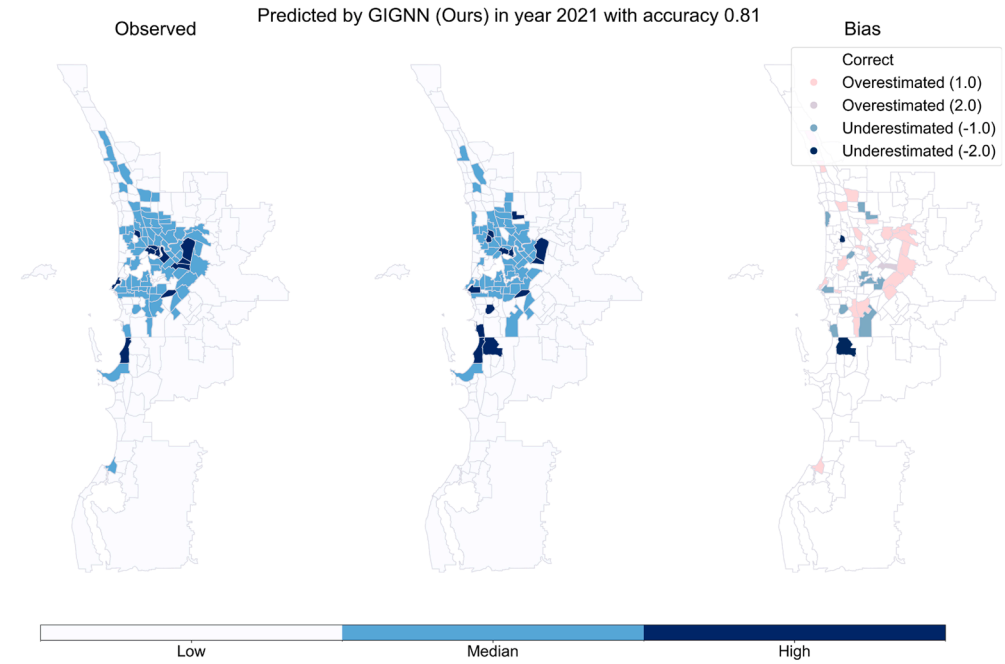

(b)

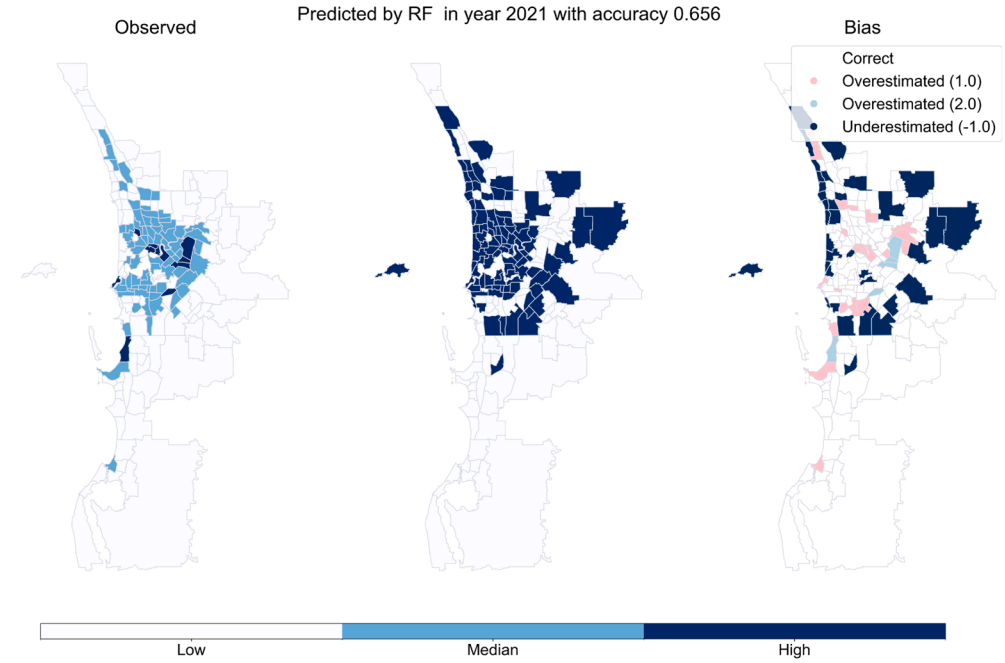

Fig. 11. Temporal generalization performance of GIGNN and RF for 2021 spatial predictions.

Table 5
GIGNN simulation performance metrics.

	Low urbanization	Median urbanization	High urbanization	Accuracy
Precision	0.845	0.867	0.692	0.841
Recall	0.933	0.712	0.818	
F1-score	0.887	0.782	0.750	
Support	105	73	11	189

6.2. Contributions

Categorical representations (e.g., 1, 2, 3) maintain SSH within the graph structure, establishing edges that denote feature-driven proximity. In contrast to standard spatial statistics models that depend on geometric distance, GIGNN constructs a multi-dimensional spatial weights matrix based on feature dissimilarity. This approach allows adjacent units with similar features to display stronger spatial interactions, whereas units with differing features interact less during feature updates. Furthermore, GIGNN improves GraphSAGE's feature aggregation by adding SSH-aware constraints. When updating nodes, feature propagation is dynamically adjusted according to the categorical differences among neighboring units. This strategy reflects real-world spatial processes, where interactions decrease with distance and greater feature divergence. Consequently, GIGNN effectively captures complex spatial dependencies, especially in situations characterized by significant stratified heterogeneity, surpassing both traditional non-graph and graph-based models in both accuracy and interpretability.

6.3. Limitations

Our model's performance is advantageous in scenarios with complex spatial dependencies (such as hexagonal grid structures). However, it faces limitations in simpler topological configurations or when spatial lag effects are diminished. Specifically, the model relies on the spatial heterogeneity of dependent and independent variables to construct the graph and quantify node and edge features. Model's k-order neighborhood aggregation mechanism (default 2nd order) may mismatch the spatial lag order of geographic units, leading to over-aggregation of multi-scale neighbor attributes and increased errors. This issue is exacerbated when the number of geographic units is high, resulting in reduced spatial effects and suboptimal performance compared to machine learning models like Random Forest. These limitations highlight the need for a more adaptive aggregation strategy to enhance model robustness and applicability across diverse spatial contexts. To address these limitations, we propose developing a dynamic aggregation mechanism that can adjust to varying spatial lag orders and unit densities, thereby improving the model's generalizability and performance across different spatial configurations.

7. Conclusions

This study proposes GIGNN, which integrates spatial stratified heterogeneity (SSH) through spatial discretization and feature-driven graph construction. By combining the SST framework with GraphSAGE, GIGNN advances spatial modeling by encoding SSH into graph structures via categorical feature dissimilarity, dynamically weighting neighbor aggregation based on feature divergence, and simulating real-world spatial decay effects. Simulation and case studies (e.g., Western Australia) demonstrate GIGNN's better performance, achieving 84.1 % accuracy (2016) and 81.0 % generalization accuracy (2021), while reducing spatial clustering of error. The model outperforms efficient machine learning and graph-based methods by 16.5–42.7 %, attributed to its ability to capture spatial dependencies and mitigate class imbalance. Future work will focus on developing adaptive spatial-lag aggregation mechanisms to enhance GIGNN's flexibility across diverse spatial patterns and geographical applications. Extending the framework to broader geographic contexts will enable its role in modeling complex spatial interactions for urban and environmental systems.

Disclosure statement

No potential conflict of interest was reported by the author(s).

Data availability statement (DAS)

The data supporting this study are openly accessible at figshare, with the doi:10.6084/m9.figshare.29571758.

CRediT authorship contribution statement

Xuankai Ma: Conceptualization, Data curation, Formal analysis, Investigation, Methodology, Software, Visualization, Writing – original draft, Writing – review & editing. **Zehua Zhang:** Conceptualization, Data curation, Investigation, Visualization, Validation, Writing – original draft, Writing – review & editing. **Yongze Song:** Validation, Writing – review & editing.

References

Australian Bureau of Statistics. (2023a, May-26). *Australian industry. Annual estimates of key economic and financial performance of industries in Australia, including income, expenses, profit, and capital expenditure*. https://www.abs.gov.au/statistics/industry/industry-overview/australian-industry/2021-22.

Australian Bureau of Statistics. (2023b, November-22). *Data by region methodology*. https://www.abs.gov.au/methodologies/data-region-methodology/2011-23.

Australian Bureau of Statistics. (2023c, April-20). *Regional population. Statistics about the population and components of change (births, deaths, migration) for Australia's capital cities and regions.* https://www.abs.gov.au/statistics/people/population/regional-population/latest-release.

Australian Bureau of Statistics. (2023d). *The Australian Census. the census is the most comprehensive snapshot of the country and tells the story of how we are changing.* https://www.abs.gov.au/census/about-census/australian-census.

Australian Bureau of Statistics. (2021, July 20). *Statistical area level 2. Australian statistical geography standard (ASGS) edition 3.* https://www.abs.gov.au/statistics/standards/australian-statistical-geography-standard-asgs-edition-3/jul2021-jun2026/main-structure-and-greater-capital-city-statistical-areas/statistical-area-level-2.

Barredo Arrieta, A., Díaz-Rodríguez, N., Del Ser, J., Bennetot, A., Tabik, S., Barbado, A., Garcia, S., Gil-Lopez, S., Molina, D., Benjamins, R., Chatila, R., Herrera, F., 2020. Explainable Artificial intelligence (XAI): concepts, taxonomies, opportunities, and challenges toward responsible AI. Inf. Fusion. 58, 82–115. https://doi.org/10.1016/j.inffus.2019.12.012.

Burke, J., King, S., 2021. Edge tracing using gaussian process regression. IEEe Trans. Image Process. 31, 138–148. https://doi.org/10.1109/TIP.2021.3128329.

Dikmen, M., Burns, C., 2022. The effects of domain knowledge on trust in explainable AI and task performance: a case of peer-to-peer lending. Int. J. Hum. Comput. Stud. 162, 102792. https://doi.org/10.1016/j.ijhcs.2022.102792.

Ding, Y., Zhao, X., Zhang, Z., Cai, W., Yang, N., 2021. Multiscale graph sample and aggregate network with context-aware learning for hyperspectral image classification. IEEe J. Sel. Top. Appl. Earth. Obs. Remote Sens. 14, 4561–4572. https://doi.org/10.1109/JSTARS.2021.3074469.

Fischer, M.M., Wang, J., 2011. Spatial Data analysis: Models, methods, and Techniques. Springer.

Gevaert, C.M., Belgiu, M., 2022. Assessing the generalization capability of deep learning networks for aerial image classification using landscape metrics. Int. J. Appl. Earth Obs. Geoinf. 114 (103054), 103054. https://doi.org/10.1016/j.jag.2022.103054.

Goodchild, M.F., 2004. The validity and usefulness of laws in geographic information science and geography. Ann. Assoc. Am. Geogr. 94, 300–303. https://doi.org/10.1111/j.1467-8306.2004.09402008.x.

Hu, Y., Mai, G., Cundy, C., Choi, K., Lao, N., Liu, W., Lakhanpal, G., Zhou, Z., Joseph, K., 2023. Geo-knowledge-guided GPT models improve the extraction of location descriptions from disaster-related social media messages. Int. J. Geogr. Inf. Sci. 37 (11), 2289–2318. https://doi.org/10.1080/13658816.2023.2266495.

Hamilton, W.L., Ying, Z., Leskovec, J., 2017. Inductive Representation Learning On Large Graphs, 30. ArXiv, pp. 1024–1034. https://doi.org/10.48550/arXiv.1706.02216.

Islam, M.D., Li, B., Lee, C., Wang, X.-g., 2022. Incorporating spatial information in machine learning: the Moran eigenvector spatial filter approach. Trans. GIS. 26, 902–922. https://doi.org/10.1111/tgis.12894.

Iyer, R., Li, Y., Li, H., Lewis, M., Sundar, R., Sycara, K., 2018. Transparency and explanation in deep reinforcement learning neural networks. In: Proceedings of the 2018 AAAI/ACM Conference on AI, Ethics, and Society. https://dl.acm.org/doi/pdf/10.1145/3278721.3278776.

Jiang, Z., 2020. Spatial structured prediction models: applications, challenges, and techniques. IEEe Access. 8, 38714–38727. https://doi.org/10.1109/ACCESS.2020.2975584.

J. Jin, C., Park, S., Ha, H., Lee, J., Kim, J., Hutchenreuther, J., Nara, A., 2023. Predicting households' residential mobility trajectories with geographically localized interpretable model-agnostic explanation (GLIME) Int. J. Geogr. Inf. Sci. 2597–2619. https://doi.org/10.1080/13658816.2023.2264921.

Kent, E., Challenor, P., 2006. Toward estimating climatic trends in SST. Part II: random errors. J. Atmos. Ocean. Technol. 23, 476–486. https://doi.org/10.1175/JTECH1844.1.

Li, S., Dragićević, S., Anton, F., Sester, M., Winter, S., Çöltekin, A., Pettit, C., Jiang, B., Haworth, J., Stein, A., Cheng, T., 2015. Geospatial big data handling theory and methods: a review and research challenges. ISPRS. J. Photogramm. Remote Sens. https://doi.org/10.1016/J.ISPRSJPRS.2015.10.012.

Liu, Q., Xu, H., Sha, D., Lee, T., Duffy, D.Q., Walter, J., Yang, C., 2022. Hyperspectral infrared sounder cloud detection using deep neural network model. IEEe Geosci. Remote Sens. Lett. 19, 1–5. https://doi.org/10.1109/lgrs.2020.3023683.

Liu, P., Zhao, T., Luo, J., Lei, B., Frei, M., Miller, C., Biljecki, F., 2023. Towards Human-centric digital twins: leveraging computer vision and graph models to predict outdoor comfort. Sustain. Cities. Soc. 93, 104480. https://doi.org/10.1016/j.scs.2023.104480.

Miller, H.J., 2004. Tobler's first law and spatial analysis. Ann. Assoc. Am. Geogr. 94 (2), 284–289. https://doi.org/10.1111/j.1467-8306.2004.09402005.x.

Miller, J., Franklin, J., Aspinall, R., 2007. Incorporating spatial dependence in predictive vegetation models. Ecol. Modell. 202 (3–4), 225–242. https://doi.org/10.1016/J.ECOLMODEL.2006.12.012.

Reichstein, M., Camps-Valls, G., Stevens, B., Jung, M., Denzler, J., Carvalhais, N., Prabhat, 2019. Deep learning and process understanding for data-driven Earth system science. Nature 566 (7743), 195–204. https://doi.org/10.1038/s41586-019-0912-1.

Samek, W., Montavon, G., Lapuschkin, S., Anders, C.J., Muller, K.-R., 2021. Explaining deep neural networks and beyond: a review of methods and applications. Proc. IEEe Inst. Electr. Electron. Eng. 109 (3), 247–278. https://doi.org/10.1109/jproc.2021.3060483.

Sanchez-Lengeling, B., Reif, E., Pearce, A., Wiltschko, A.B., 2021. A gentle introduction to graph Neural networks. Distill 6 (9), e33. https://doi.org/10.23915/distill.00033.

Song, Y., Kalacska, M., Gašparović, M., Yao, J., Najibi, N., 2023. Advances in geocomputation and geospatial artificial intelligence (GeoAI) for mapping. Int. J. Appl. Earth. Obs. Geoinf. 120 (2023), 103300. https://doi.org/10.1016/j.jag.2023.103300.

Swietek, A.R., Zumwald, M., 2023. Visual Capital: evaluating building-level visual landscape quality at scale. Landsc. Urban. Plan. 240 (104880), 104880. https://doi.org/10.1016/j.landurbplan.2023.104880.

Tobler, W., 2004. On the first law of geography: a reply. Ann. Assoc. Am. Geogr. 94, 304–310. https://doi.org/10.1111/j.1467-8306.2004.09402009.x.

Wang, J., Gao, B., Stein, A., 2020. The spatial statistic trinity: a generic framework for spatial sampling and inference. Environ. Model. Softw. 134, 104835. https://doi.org/10.1016/j.envsoft.2020.104835.

Wang, J., Haining, R., Zhang, T., Xu, C., Hu, M., Yin, Q., Li, L., Zhou, C., Li, G., Chen, H., 2022. Statistical modeling of spatially stratified heterogeneous data. Ann. Am. Assoc. Geogr. 114, 499–519. https://doi.org/10.1080/24694452.2023.2289982.

Wang, J., Biljecki, F., 2022. Unsupervised machine learning in urban studies: a systematic review of applications. Cities. 129 (103925), 103925. https://doi.org/10.1016/j.cities.2022.103925.

Wang, Z., Brenning, A., 2023. Unsupervised active–transfer learning for automated landslide mapping. Comput. Geosci. 181 (105457), 105457. https://doi.org/10.1016/j.cageo.2023.105457.

Wu, Z., Pan, S., Chen, F., Long, G., Zhang, C., Yu, P.S., 2020. A comprehensive survey on graph neural networks. IEEe Trans. Neural Netw. Learn. Syst. 32 (1), 4–24. https://doi.org/10.1109/TNNLS.2020.2978386.

Xing, J., Sieber, R., 2023. The challenges of integrating explainable artificial intelligence into GeoAI. Trans. GIS. 27 (3), 626–645. https://doi.org/10.1111/tgis.13045.

Xu, C., Li, F., Xia, J., 2023. Fusing high-resolution multispectral image with trajectory for user next travel location prediction. Int. J. Appl. Earth Obs. Geoinf. 116 (103135), 103135. https://doi.org/10.1016/j.jag.2022.103135.

Zhang, Z., Song, Y., Luo, P., Wu, P., 2023. Geocomplexity explains spatial errors. Int. J. Geogr. Inf. Sci. 37 (7), 1449–1469. https://doi.org/10.1080/13658816.2023.2203212.

Zhang, Z., Song, Y., Wu, P., 2022. Robust geographical detector. Int. J. Appl. Earth. Obs. Geoinf. 109 (102782), 102782. https://doi.org/10.1016/j.jag.2022.102782.

Zhang, Z., Li, Z., Song, Y., 2024a. On ignoring the heterogeneity in spatial autocorrelation: consequences and solutions. Int. J. Geogr. Inf. Sci. https://doi.org/10.1080/13658816.2024.2391981.

Zhang, Z., Song, Y., Karunaratne, L., Wu, P., 2024b. Robust interaction detector: a case of road life expectancy analysis. Spat. Stat. 59, 100814. https://doi.org/10.1016/j.spasta.2024.100814.

Zhu, D., Liu, Y., Yao, X., Fischer, M.M., 2022. Spatial regression graph convolutional neural networks: a deep learning paradigm for spatial multivariate distributions. Geoinformatica 26 (4), 645–676. https://doi.org/10.1007/s10707-021-00454-x.

Zhu, D., Zhang, F., Wang, S., Wang, Y., Cheng, X., Huang, Z., Liu, Y., 2020. Understanding place characteristics in geographic contexts through graph convolutional neural networks. Ann. Am. Assoc. Geogr. 110 (2), 408–420. https://doi.org/10.1080/24694452.2019.1694403.